Practical Characterization of the Effect of the Transmission Carrier Phases in Passive Intermodulation

Davide Smacchia, Pablo Soto, *Member, IEEE*, Vicente E. Boria, *Fellow, IEEE*, Òscar Monerris, Javier Ossorio, David Raboso, José Vicente Morro, and Mónica Martínez-Mendoza

***Abstract*— The effect of the phase of the input carriers has been traditionally neglected in the characterization of passive intermodulation (PIM) since standard two-tone PIM tests seem to be unaffected by phase variations of the excitation signals. However, the phase of the input carriers can be of relevance in many practical applications. This article is aimed at filling this gap in the technical literature. First, the existing theory explaining why the phases do not affect the measured PIM contribution for a two-carrier excitation but can be of relevance for generic multicarrier scenarios is summarized. PIM measurements for complex signals composed of several carriers with varying phases are then reported, enabling the practical characterization of this effect for the first time. Experimental results of the test campaigns are fully aligned with theoretical predictions, thus allowing us to identify those PIM contributions that can be affected by the carrier phases and assess the expected variation range in their amplitude level.**

***Index Terms*— Carrier phase, intermodulation distortion, microwave measurements, multicarrier systems, passive circuits, satellite communications.**

I. Introduction

PASSIVE intermodulation (PIM) interference has been a well-known issue for the space industry since the 1970s [1], [2]. The simultaneous operation of satellite payloads in both transmission (downlink) and reception (uplink) at different frequency bands, together with the high transmitted radio frequency (RF) power levels and number of carriers at the downlink, stimulate PIM generation. Undesired PIM terms generated in the downlink may fall in the reception band and interfere with the weak signals to be received, thus reducing (or even endangering, in extreme cases) the uplink performance [3], [4].

The continuous increase in number of channels and link capacity in modern satellites are, in fact, fostering PIM issues [5], [6], [7]. This is even further critical in high-throughput satellite (HTS) payloads operating at higher frequency bands to meet throughput demands [8], [9]. Indeed, higher operational frequencies lead to a wavelength reduction, with a consequent increase in the surface current density, a typical PIM ignition factor [10], [11], [12], [13].

The intrinsic nature of passive intermodulation (PIM), usually linked to imperfections in metal-to-metal contacts and workmanship quality, makes extremely difficult the development of reliable prediction tools. Therefore, PIM characterization and qualification must rely on experimental verification of the involved hardware [5], [14]. The standard PIM test is based on two equal-amplitude continuous-wave (CW) input tones [15], [16], as the complexity of the test bench highly increases with the number of excitation signals to be mixed and applied simultaneously to the device under test (DUT).

In the usual two-tone testing scenario, however, the level of the PIM term, when present, has been observed to be independent of the carrier phases. Its measured level is kept over time despite the slow phase drift that may suffer from the high-power amplifiers (HPAs) during their heating-up or the one associated with the signal generators. This has led to ignoring the effect of the phases in PIM testing, which are assumed to be zero for the sake of simplicity [17]. However, the effect of the phases for a generic multicarrier excitation should be analyzed in more detail. This is indeed the case of typical payload scenarios, in which the transmission channels are equally spaced in the frequency domain [18] by using frequency division multiplexing (FDM) or similar schemes [19].

Although this effect has been already studied for active intermodulation (AIM) [20], the practical characterization for PIM, however, has not been accomplished before, due to the complexity of the required PIM measurement test benches. Nevertheless, this experimental validation is indeed required to be able to extend such results to PIM.

In this article, the effect of the carrier phases in PIM for multicarrier scenarios is addressed. First, the general theory traditionally used in AIM for both noncommensurate and

Manuscript received 15 December 2023; revised 2 March 2024 and 26 March 2024; accepted 9 April 2024. Date of publication 23 April 2024; date of current version 7 October 2024. This work was supported in part by the Ministerio de Ciencia e Innovación, MCIN/AEI/10.13039/501100011033, Spanish Government, under Research and Development under Grant PID2022-136590OB-C41 and Grant TED2021-129196B-C41; and in part by European Space Agency (ESA) through several Research and Development activities. *(Corresponding author: Pablo Soto.)*

Davide Smacchia, Òscar Monerris, and Javier Ossorio are with ESA-VSC European High Power RF Space Laboratory, E-46022 Valencia, Spain (e-mail: davide.smacchia@val-space.com; oscar.monerris@val-space.com; javier.ossorio@val-space.com).

Pablo Soto, Vicente E. Boria, José Vicente Morro, and Mónica Martínez-Mendoza are with iTEAM, Universitat Politècnica de València, E-46022 Valencia, Spain (e-mail: pabsopac@dcom.upv.es; vboria@dcom.upv.es; jomorros@dcom.upv.es; momarmen@iteam.upv.es).

David Raboso is with the European Space Research and Technology Center of the European Space Agency (ESTEC-ESA), 2200 AG Noordwijk, The Netherlands (e-mail: david.raboso@esa.int).

Color versions of one or more figures in this article are available at https://doi.org/10.1109/TMTT.2024.3389461.

Digital Object Identifier 10.1109/TMTT.2024.3389461

commensurate scenarios is revisited, demonstrating that for the two-tone case (the standard one for testing), the role of the phases of the transmission carriers can be neglected. Next, the measurement of the power level of PIM signals originating from two or more carriers, with varying phases, is addressed. The results from two multicarrier test campaigns studying the impact of the carrier phases on the power level of PIM spectral components are reported, allowing the practical characterization of this effect for the first time. An excellent agreement between experimental results and predictions is obtained, thus validating the theoretical model also for PIM.

II. Theory

A. Noncommensurate Scenario

In a generic multicarrier scenario under the noncommensurate assumption, the carriers are chosen in such a way that at a given frequency only falls one PIM term. Let us first study the effect of the phase of the carriers under this scenario by means of the classic nonlinear theory.

Consider a generic PIM term with amplitude A_{PIM} and phase Φ_{PIM} at an angular frequency ω_{PIM}. The PIM contribution at this particular angular frequency can be modeled as

$$V_{\text{PIM, NC}}(t) = \Re\left\{\left(A_{\text{PIM}}e^{j\Phi_{\text{PIM}}}\right)e^{j\omega_{\text{PIM}}t}\right\} \tag{1}$$

with A_{PIM}, Φ_{PIM}, and ω_{PIM} being real numbers.

Note that the phase of the carriers is assumed to have a very slow time variation when compared to the RF signal and the integration time of the spectrum analyzer, and, therefore, can be treated as constant here. This is clearly the situation for the phase drift of the HPAs or the signal generators. The associated mean PIM power at ω_{PIM} is

$$P_{\text{PIM,NC}} = \frac{1}{2Z_0}\left|A_{\text{PIM}}e^{j\Phi_{\text{PIM}}}\right|^2 = \frac{A_{\text{PIM}}^2}{2Z_0} \tag{2}$$

being independent of the phase of the carriers, which do not play a significant role in the measured level of the intermodulation term in noncommensurate scenarios.

The classic two-tone PIM tests [15] are a representative case of this class of scenarios. Let us consider an excitation composed of two generic input carriers having different phases with a slow time variation. On a nonlinear system with only third-order PIM contributions, the ignited PIM is known to be composed of the terms falling at angular frequencies ω_1, ω_2, $3\omega_1$, $3\omega_2$, $2\omega_1 \pm \omega_2$, and $2\omega_2 \pm \omega_1$. The most problematic in many satellite payloads is normally the one at $2\omega_2 - \omega_1$, due to its closeness to the carrier frequencies. The voltage associated with this PIM contribution is given by [20]

$$V_{3-2}(t) = \gamma\frac{3}{4}A_1A_2^2\cos[(2\omega_2 - \omega_1)t + 2\Phi_2(t) - \Phi_1(t)] \tag{3}$$

where the subindex 3-2 denotes the third-order PIM contribution for a two-carrier scenario, and γ is the coefficient of the third-order term of the polynomial expansion modeling the nonlinear system.

For CW input signals, the phases of the carriers vary extremely slowly when compared with the integration period T of the spectrum analyzer, which covers several cycles of the RF carriers (so that the average value is obtained regardless of the starting and ending point of the integration interval). As a result, they can be considered as constants $\Phi_1(t) = \Phi_1$ and $\Phi_2(t) = \Phi_2$, and the mean power level is measured

$$P_{3-2}(t) = \left(\frac{3}{4}\right)^2\frac{\left(\gamma A_1A_2^2\right)^2}{2Z_0}. \tag{4}$$

As it can be observed in (4), the power associated with this particular term is independent of the phase of each carrier, demonstrating that in the two-tone scenario traditionally used for PIM testing, such phases do not affect to the measured level of the PIM term. This result, which is experimentally verified in Section III, has led to neglect the effect of the carrier phases in PIM.

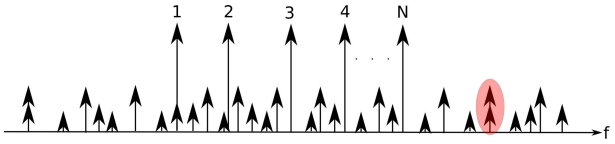

Fig. 1. Multicarrier scenario in which two different PIM tones fall at the same frequency.

B. Commensurate Scenario

In the commensurate case, more than one PIM contribution falls at a given frequency (see Fig. 1). In this scenario, the overall PIM contribution at the angular frequency ω_{PIM} can be generalized in the form

$$V_{\text{PIM,C}}(t) = \Re\left\{\sum_{i=1}^{P}\left(A_{\text{PIM},i}e^{j\Phi_{\text{PIM},i}}\right)e^{j\omega_{\text{PIM}}t}\right\} \tag{5}$$

where $A_{\text{PIM},i}$ and $\Phi_{\text{PIM},i}$ are real numbers representing, respectively, the amplitude and phase of the ith individual PIM term originated at ω_{PIM}.

It is assumed again that the phase of the carriers is nearly constant along the integration time of the spectrum analyzer, due to its slow time variation. As a result, the associated mean PIM power measured at ω_{PIM} can be expressed as

$$\begin{aligned} P_{\text{PIM},C} &= \frac{1}{2Z_0}\left|\sum_{i=1}^{P}\left(A_{\text{PIM},i}e^{j\Phi_{\text{PIM},i}}\right)\right|^2 \\ &= \frac{1}{2Z_0}\left(\sum_{i=1}^{P}\left[A_{\text{PIM},i}^2 + \sum_{j=i+1}^{P}2A_{\text{PIM},i}A_{\text{PIM},j}\cos\left(\Phi_{\text{PIM},j} - \Phi_{\text{PIM},i}\right)\right]\right). \end{aligned} \tag{6}$$

Note, how in this case, the phase difference between the different PIM contributions overlapping at ω_{PIM}, $\Delta\Phi_{j,i} = \Phi_{\text{PIM},j} - \Phi_{\text{PIM},i}$, has a relevant effect on the mean power level of the overall PIM component at such a frequency. The maximum value is obtained when all PIM contributions are in phase, resulting in a voltage summation

$$P_{\text{PIM}} \propto \left(\sum_{i=1}^{P}A_{\text{PIM},i}\right)^2 \tag{7}$$

TABLE I
INFLUENCE OF THE CARRIER PHASES FOR TWO PIM TERMS FALLING AT THE SAME FREQUENCY, COMPARED WITH ONLY ONE CONTRIBUTION OF AMPLITUDE $A_{\mathrm{PIM},1}$

$A_{\mathrm{PIM},2}/A_{\mathrm{PIM},1}$	Max. power	Min. power	Fluctuation range
0	0 dB	0 dB	0 dB
1/10	+0.83 dB	−0.92 dB	1.74 dB
1/4	+1.94 dB	−2.50 dB	4.44 dB
1/2	+3.52 dB	−6.02 dB	9.54 dB
1	+6.02 dB	$-\infty$ dB	∞ dB
2	+9.54 dB	0 dB	9.54 dB
4	+13.98 dB	+9.54 dB	4.44 dB
10	+20.83 dB	+19.08 dB	1.74 dB

whereas the best case occurs when the terms are combined in such a way that the amplitude of the PIM resultant is minimized.

Therefore, in a commensurate scenario, the phases of the carriers play a relevant role in the PIM level. As a result, a variation in the carrier phases (especially, relatively slow variations) may cause a severe fluctuation along the time in the PIM level reading provided by the spectrum analyzer. This is a completely different situation to the standard two-tone testing, where the PIM reading is more stable (as discussed in Section II-A).

Table I represents the potential fluctuation range for the particular case where a second PIM term, of amplitude $A_{\mathrm{PIM},2}$, falls at the same frequency of a term of amplitude $A_{\mathrm{PIM},1}$. In this case, the PIM power level can be between $(A_{\mathrm{PIM},1} + A_{\mathrm{PIM},2})^2/2Z_0$ and $|A_{\mathrm{PIM},1} - A_{\mathrm{PIM},2}|^2/2Z_0$, depending on the phase difference between both terms. As can be observed, the variation range increases as the amplitudes of both PIM contributions become more similar. The worst case occurs when the amplitudes of the two terms are the same so that the PIM power can oscillate between a fourfold increase or a complete cancellation with respect to the noncommensurate case. Conversely, as one PIM term becomes more predominant over the other, the fluctuation range decreases rapidly.

In a general multicarrier scenario, since the amplitude of the PIM terms decays with the PIM order [17], [21], [22], [23], the higher fluctuation is normally observed when several PIM terms of the same or very similar orders fall at the same frequency. In Section III, some examples are considered and verified with experimental data.

III. MEASUREMENTS

The intermodulation from passive microwave hardware not including intrinsically nonlinear materials (such as ferrites) is mainly due to small-scale imperfections in metal-to-metal contacts. Since the accurate modeling of these defects is extremely difficult, the practical characterization of PIM is based on experimental measurements.

Conducted PIM measurements, however, require complex test beds even for the usual two-tone standard excitation [24], which must be carefully assembled. Once the different signals are combined, the residual intermodulation generated by the bench itself should not interfere with the weak PIM signals to be detected. Moreover, specific hardware with outstanding performance is required in such test beds [24], [25]. These are the reasons why PIM is normally measured by injecting only two

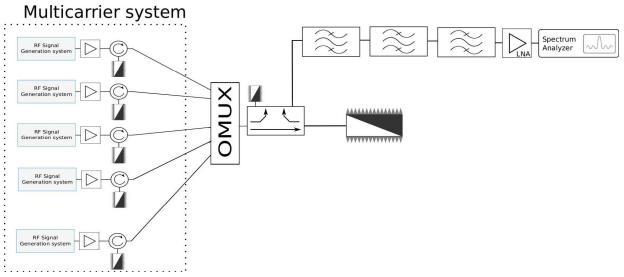

Fig. 2. Schematic of the PIM measurement setup based on the multicarrier facility, able to combine up to five high-power carriers at once.

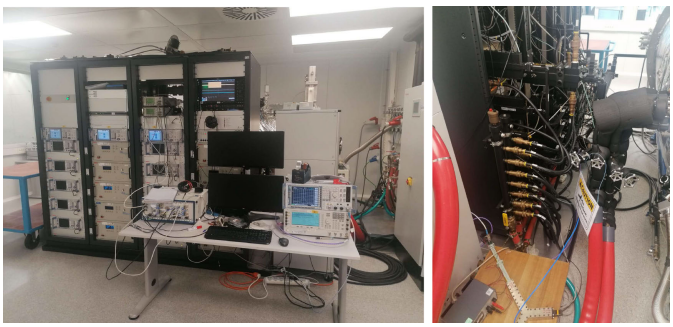

Fig. 3. Assembled PIM setup based on the multicarrier facility for the first set of PIM measurements.

carriers at the DUT input. Note that PIM measurement setups are considerably more intricate than AIM ones, due to the subtle signals to be measured (power levels below −180 dBc are not uncommon for satellite applications). In fact, a PIM test bed must also be free of AIM, as the later nonlinear degradation is much more powerful than PIM.

The effect to be characterized in this article requires combining a larger number of carriers with varying phases. The carriers must be amplified separately before being combined, to avoid AIM in the HPAs. From the authors' knowledge, only the works in [21] and [26] provide properly measured PIM data for waveguide satellite hardware in multicarrier scenarios. In [26], a high-performance C-band quadriplexer is used to combine three carriers and measure the reflected PIM according to the principles described in [25]. On the other hand, in [21], the PIM terms are measured at the spacecraft level using the payload of the on-flight satellite. Unfortunately, this cannot be performed in a laboratory test.

In this work, the philosophy proposed in [25] for PIM measurements has also been followed. It consists of using low-PIM multiplexers to combine the carriers, limiting the number of flanged interconnections to avoid potential sources of residual PIM. The high-power multiplexer of the ESA-VSC European High Power RF Space Laboratory multicarrier facility has been used to successfully mix the carriers, which have been amplified independently before. The resulting test bed provided an outstanding noise PIM floor of about −150 dBm for 100 W CW input carriers.

Two main sets of measurements were conducted, as detailed in Sections III-A and III-B. The first set of measurements was focused on third-order PIM in reduced multicarrier scenarios, which were particularly conceived for validating the theory summarized in Section II. Then, a more complex set of measurements was performed with a multicarrier excitation having

TABLE II

FREQUENCY OF THE INPUT CARRIERS AND THE MEASURED PIM SIGNAL, TEST SCENARIO A.1

Carriers				PIM	
f_1 [GHz]	f_2 [GHz]	f_3 [GHz]	f_4 [GHz]	order	f_{PIM} [GHz]
10.7135	10.8125	11.1095	11.2085	3	11.6045

TABLE III

THIRD-ORDER PIM FLUCTUATION DUE TO CARRIER PHASE VARIATION IN UNEQUAL AMPLITUDE PIM TERMS, TEST SCENARIO A.1

Carriers				PIM		
f_1	f_2	f_3	f_4	PIM term	Max [dBm]	Min [dBm]
–	⊗	–	×	$2f_4 - f_2$	−138.2	−138.4
×	–	×	⊗	$f_4 + f_3 - f_1$	−133.3	−133.5
×	⊗	×	×	$f_4 + f_3 - f_1$ $2f_4 - f_2$	−130.2	−139.5

× activated carrier – carrier not activated
⊗ activated carrier with phase swept from 0° to 360°

TABLE IV

FREQUENCY OF THE INPUT CARRIERS AND THE MEASURED PIM SIGNAL, TEST SCENARIO A.2

Carriers				PIM	
f_1 [GHz]	f_2 [GHz]	f_3 [GHz]	f_4 [GHz]	order	f_{PIM} [GHz]
10.8125	11.0105	11.1095	11.2085	3	11.6045

TABLE V

THIRD-ORDER PIM FLUCTUATION DUE TO CARRIER PHASE VARIATION IN EQUAL AMPLITUDE PIM TERMS, TEST SCENARIO A.2

Carriers				PIM		
f_1	f_2	f_3	f_4	PIM term	Max [dBm]	Min [dBm]
–	⊗	–	×	$2f_4 - f_2$	−138.0	−138.0
×	⊗	×	×	$2f_4 - f_2$ $2f_3 - f_1$	−132.2	≤ -150 (*)

× activated carrier – carrier not activated
⊗ activated carrier with phase swept from 0° to 360°
(*) −150 dBm was the residual noise floor of the PIM facility

up to seven carriers delivered at once, where several PIM contributions of the same and different orders can interfere at the same frequency.

A. Reduced Multicarrier Scenarios—Third-Order PIM

For this first set of measurements, several cases with four and five transmission carriers have been checked experimentally by conducting practical measurements in the Ku-band. The multicarrier facility available at the ESA-VSC European High Power RF Space Laboratory facility has been adapted for third-order PIM (the most critical one) evaluation. A schematic of the test bed is depicted in Fig. 2, where five carriers are combined by an output high-power multiplexer and injected into a load acting as a PIM source. The reflected PIM contribution is routed through a directional coupler to a filter bank and, after being amplified, is detected using a spectrum analyzer. As the test bench components are not ideal, a portion of the high-power input carriers is coupled to the PIM branch. The filter bank of this branch, however, is conceived to let the PIM signal pass through and provide high rejection in the transmission band. As a result, the amount of power of the input carriers arriving at the reception port is so small that the AIM generated in the low noise amplifier (LNA) is negligible and unable to mask the PIM signal to be measured. Fig. 3 shows some pictures of the assembled test set-up. Three test scenarios with up to five CW carriers of the same amplitude (100 W each) were considered. In each scenario, the carriers were switched ON or OFF depending on the particular PIM measurement to be carried out.

1) Test Scenario A.1: Two third-order PIM terms at the same frequency with different amplitude factors.

The first test scenario is detailed in Tables II and III. It corresponds to a four-carrier case where the frequency of the fourth carrier, f_4, is set to $f_3 + f_2 - f_1$. As a result, since $2f_4 - f_2 = f_4 + f_3 + f_2 - f_1 - f_2 = f_4 + f_3 - f_1$, the two third-order PIM contributions at $f_4 + f_3 - f_1$ and $2f_4 - f_2$ fall at the same frequency, in this case of value $f_{\text{PIM}} = 11.6045$ GHz. Note that, theoretically, the amplitude of the PIM term at $2f_4 - f_2$ is half of the value for the term at $f_4 + f_3 - f_1$ [27].

As spotted in Table III, several tests were performed activating two, three, or four carriers. The activated carriers are denoted with a cross mark. For each test, the phase of one of the carriers was swept from 0° to 360° (circled cross mark), and the highest and lowest detected PIM levels were recorded. Note that the amplitudes and phases of the different PIM terms cannot be easily controlled (due to the intrinsic nature of PIM). As a result, the more straightforward way to measure the amplitude variation range of the PIM contribution at a particular frequency is by varying the phase of one of the involved transmission carriers.

For the first two tests, only one PIM term falls at f_{PIM}. The PIM power was not affected by the phase variation of the carriers in these two tests, as predicted by the theory (see the first row of Table I). Note also how the level of the PIM term corresponding to the mixing of three carriers (i.e., $f_4+f_3-f_1$) is around 5 dB higher than the one associated with mixing two carriers (i.e., $2f_4 - f_2$), which is close to the theoretical value of 6 dB [26], [27]. The slight discrepancy can be attributed to the PIM energy conservation law [27], or small inaccuracies in the PIM setup (errors in PIM readings of about ±1 dB in a spectrum analyzer are not uncommon).

On the other hand, for the third test case, where two PIM terms were beating at the same frequency, the phase variation in the carrier at f_2 caused a fluctuation of the PIM level between +3.1 dB (worst case) and −6.0 dB (best case) when compared with the isolated PIM term at $f_4+f_3-f_1$, resulting in an overall variation of 9.3 dB for the extreme measured values reported in Table III. These results are in full agreement with the ones theoretically predicted in the fourth row of Table I, as this case corresponds to a ratio of 1/2 between the amplitude of the second PIM contribution (the one at $2f_4-f_2$) and the reference PIM contribution not affected by the phase sweep (the one at $f_4 + f_3 - f_1$).

2) Test Scenario A.2: Two third-order PIM terms at the same frequency with equal amplitude factors.

The second test scenario is detailed in Tables IV and V. For this particular case, f_4 is equal to $f_3+(f_2-f_1)/2$, so that the PIM terms at $2f_3 - f_1$ and $2f_4 - f_2$ coincide in frequency.

The second scenario corresponds to the case where both PIM terms falling at the same PIM frequency have the same

TABLE VI

FREQUENCY OF THE INPUT CARRIERS AND THE MEASURED THIRD-ORDER PIM SIGNAL, TEST SCENARIO A.3

Carriers					PIM
f_1 [GHz]	f_2 [GHz]	f_3 [GHz]	f_4 [GHz]	f_5 [GHz]	f_{PIM} [GHz]
10.7135	11.0105	11.1095	11.2085	11.3075	11.6045

TABLE VII

THIRD-ORDER PIM FLUCTUATION DUE TO CARRIER PHASE VARIATION IN UNEQUAL AMPLITUDE PIM TERMS, TEST SCENARIO A.3

Carriers					PIM		
f_1	f_2	f_3	f_4	f_5	PIM term	Max [dBm]	Min [dBm]
–	⊗	–	–	×	$2f_5 - f_2$	−138	−138
×	–	⊗	×	–	$f_4 + f_3 - f_1$	−132	−132
×	⊗	×	×	×	$f_5 + f_2 - f_1$ $f_4 + f_3 - f_1$ $2f_5 - f_2$	−126	−138

× activated carrier – carrier not activated
⊗ activated carrier with phase swept from 0° to 360°

amplitude, as shown in the fifth row of Table I. As a result, its combination can range between a PIM power increase of +6 dB and a total cancellation, when compared to the presence of only one of the PIM terms. The experimental results shown in Table V are again in line with the theoretical predictions of the simple model for commensurate scenarios reported in Section II.

3) Test scenario A.3: Three third-order PIM terms at the same frequency with different amplitude factors.

For this particular case, five transmission carriers are chosen in such a way that three third-order PIM terms fall at the same PIM frequency, two of the type $\pm f_i \pm f_j \pm f_k$ and one of the type $2f_i - f_j$. This test scenario is summarized in Tables VI and VII.

The first and second rows of Table VII prove again the irrelevance of the phase of the carriers in the measured PIM level when only one contribution is present. Particularly interesting, however, is the third row of Table VII, where the presence of three PIM terms having different amplitude causes a 12-dB fluctuation. The worst case (i.e., higher PIM) should be observed when the three PIM terms are combined in phase maximizing the PIM resultant. The phase variation of the carrier at f_2 allows to modify the phases of the PIM contributions at $f_5 + f_2 - f_1$ and $2f_5 - f_2$, but the phase delta between these two terms is unknown. Anyway, the worst PIM situation should be close to the case where the higher amplitude contributions at $f_5 + f_2 - f_1$ and $f_4 + f_3 - f_1$ add in phase. In fact, the maximum PIM is 6 dB higher than the isolated term at $f_4 + f_3 - f_1$, as shown in Table VII. Conversely, the lowest PIM should be close to the one obtained in the case where the two terms with higher amplitude cancel out. Comparing the first and last row of Table VII, it can be observed how the minimum PIM power measured has the same value of the isolated term at $2f_5 - f_2$.

The obtained experimental results in the three test scenarios fully validate the theory summarized in Section II for PIM. The analysis has been focused only on third-order PIM contributions, although more PIM terms are indeed present. An in-house code developed in MATLAB [28] has, in fact, revealed the presence of three PIM terms of third order,

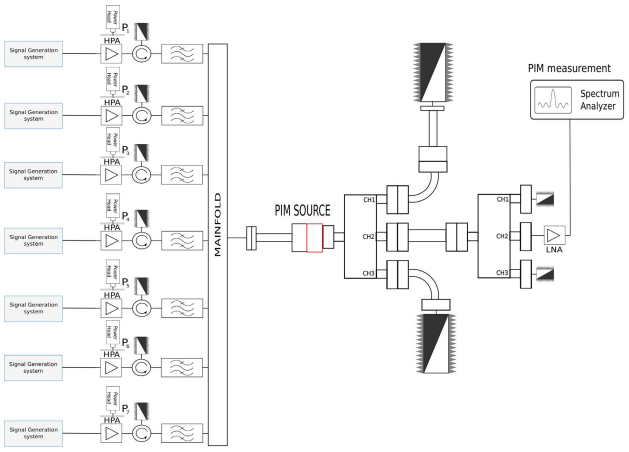

Fig. 4. Schematic of the PIM measurement setup based on the multicarrier facility, able to combine up to seven high-power carriers at once.

Fig. 5. Assembled PIM setup based on the multicarrier facility for the enhanced multicarrier scenario.

eight of fifth order, and 18 terms with order seventh at the PIM frequency $f_{\text{PIM}} = 11.6045$ GHz considered for the test scenario A.3. However, the amplitude level of the fifth-order PIM contributions tend to be at least 15 dB lower than the third PIM order terms [22] and might only slightly affect the overall PIM level when third-order PIM terms are present (anyway, this can be one of the main causes behind the slight discrepancies with regard to the theoretical predictions). The effect of the seventh-order PIM contributions should even be less noticeable in this particular case.

B. Enhanced Multicarrier Scenario—Several Odd PIM Orders

For the second set of measurements, several test cases from two up to seven CW transmission carriers have been checked experimentally. Also in this case, the Ku-band multicarrier facility available at the ESA-VSC European High Power RF Space Laboratory was used and adapted to measure third, fifth, and seventh PIM orders. The overall amount of RF power within the system was set to 100 W CW (i.e., 33.3 W per carrier for a three-carrier scenario), thus diminishing even more the PIM noise floor with respect to the reduced multicarrier scenarios in Section III-A. A schematic of the test bed is depicted in Fig. 4, where seven carriers are combined by the high-power output multiplexer. Then, the transmission carriers are split from the PIM signal by a low PIM triplexer. Additional filtering is incorporated in the PIM branch, to avoid AIM in the LNA, which could mask the effective PIM signal. The waveguide flange bolted connection between the multicarrier facility (idirite-coated) and the low PIM triplexer (silver-coated) is assumed to be the main PIM

TABLE VIII
PIM TEST SCENARIOS FOR THE SECOND SET OF MEASUREMENTS

Test case	Number of carriers	Number of PIM terms				
		3^{rd} order	5^{th} order	7^{th} order	9^{th} order	11^{th}–15^{th} order
1	2	1	–	–	–	–
2	3	1	–	–	–	–
3	2	–	1	–	–	–
4	3	–	1	–	–	–
5	4	–	1	2	–	2
6	5	–	1	–	3	8
7	2	–	–	1	–	–
8	3	–	–	1	–	–
9	4	–	–	1	–	1
10	5	–	2	5	–	–
11	6	–	–	7	–	–
12	7	–	1	16	–	–

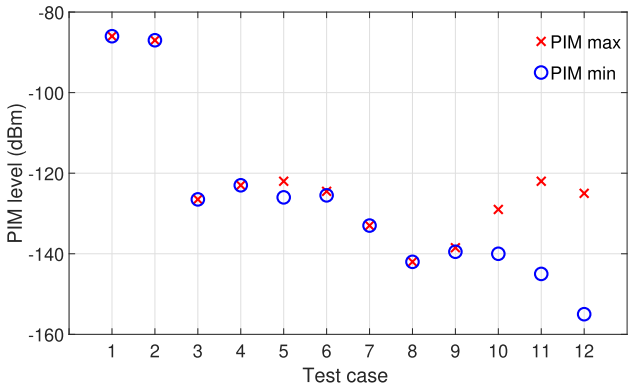

Fig. 6. Test results from the second set of measurements for each test case described in Table VIII.

source within the system [24]. The conducted forward PIM signal is evaluated. Some photographs of the resulting test facility are provided in Fig. 5.

Twelve test cases involving a different number of carriers and PIM orders were considered, as detailed in Table VIII. For each test scenario, the carriers were switched ON or OFF depending on the particular PIM measurement carried out. As it can be observed in the last column of Table VIII, only the cases with four or more input carriers have several PIM contributions coinciding at the PIM frequency under consideration. This was checked by the dedicated software developed in MATLAB [28], which allows to determine all the combinations in the form $|\pm m_i \pm n_j \pm \cdots \pm r_k|$, where $\text{PIM}_{\text{order}} = m_i + n_j + \cdots + r_k$ [17], [29].

For each test scenario, the phase of one of the carriers was swept from 0° to 360° by the signal synthesizer, emulating a phase drift of the corresponding HPA. The results from this set of measurements are summarized graphically in Fig. 6, where the maximum and the minimum measured PIM levels are plotted. Similar to the first set of measurements (see Section III-A), and despite the phase variation on one of the transmission carriers, the measured level was almost constant when only one PIM term is present at the measured PIM frequency. Conversely, a fluctuation is observed when several PIM tones were beating at the PIM frequency of interest. In the test scenarios 5, 6, and 9 of Table VIII, there is only one main PIM contribution, but also a few additional contributions of higher odd-orders, resulting in a slight fluctuation in the measured PIM level with the varying phase of one of the involved carriers. Equation (6) may explain this fluctuation, as the amplitude ratio between PIM terms increases with the difference in the PIM order [17], [22]. In test cases 10–12, on the other hand, the high number of input carriers leads to a larger number of terms at the PIM frequency of the main order or of the next higher odd order. In test case 12, although only one fifth-order PIM term is present, a total number of 16 contributions of the seventh order coincide at the same PIM frequency. Due to the large number of PIM contributions of the same or similar odd order coinciding at the same frequency, the proposed theory would also explain the huge fluctuations (above 10 dB) observed in the measured PIM level in these particular cases.

IV. CONCLUSION

In this article, the effect of the phases of the transmission carriers in PIM has been studied.

First, two different scenarios have been distinguished: the noncommensurate case where the carriers are chosen in such a way that only one PIM term falls within a given frequency, and the commensurate case where several PIM contributions coincide at the same frequency. A theoretical summary of the mathematical modeling for these two scenarios has been presented. According to this theory, when several PIM contributions overlap at the same frequency (i.e., the commensurate scenario), the mean power of the overall PIM term is affected by the phase difference between carriers.

A novel PIM test bench, able to mix several carriers with varying phases, has been successfully implemented. As a result, this effect has been characterized in practice. Measurements show an excellent match with theoretical predictions for the reduced cases of only one, two, or three PIM terms of third-order beating at the same frequency. For a multicarrier scenario where a large number of terms are ignited at the considered PIM frequency, amplitude fluctuations were observed when a phase sweep on one of the transmission carriers was applied. The fluctuations were particularly relevant when several PIM terms belonging to the same or next odd order were present at the same frequency. However, the range of these variations is not straightforward to determine analytically, given the large number of terms playing a role in the resultant PIM vector. In any case, the observed fluctuation might be explained by the theoretical model.

In conclusion, the phase of the carriers must be carefully taken into account for testing in PIM scenarios where several PIM terms coincide at the same frequency (a usual situation, in practice, in systems with several channels equally spaced in frequency). This is a significant difference with the standard two-carrier scenario [15], where the measured PIM level is essentially independent of the carrier phases, which has led to neglect the effect of such phases in PIM characterization.

ACKNOWLEDGMENT

The authors would like to acknowledge the ESA-VSC European High Power RF Space Laboratory for its contribution to this work, A laboratory funded by the European Regional Development Fund, a way of making Europe.

REFERENCES

[1] J. G. Dumolin, "Passive intermodulation and its effect on space programs," in *Proc. IEE Colloq. Screening Effectiveness Meas.*, London, U.K., May 1998, pp. 1–10.

[2] C. Hoeber, D. Pollard, and R. Nicholas, "Passive intermodulation product generation in high power communications satellites," in *Proc. 11th Commun. Satell. Syst. Conf.*, San Diego, CA, USA, Mar. 1986, pp. 361–365.

[3] F. Carducci, "Passive intermodulations aspects on italsat F2/EMS spacecraft," in *Proc. Symp. Antenna Technol. Appl. Electromagn.*, Aug. 1994, pp. 377–380.

[4] J. W. Boyhan, H. F. Henzing, and C. Koduru, "Satellite passive intermodulation: Systems considerations," *IEEE Trans. Aerosp. Electron. Syst.*, vol. 32, no. 3, pp. 1058–1064, Jul. 1996.

[5] R. J. Cameron, C. M. Kudsia, and R. R. Mansour, *Microwave Filters for Communication Systems: Fundamentals, Design and Applications*, 2nd ed. Hoboken, NJ, USA: Wiley, 2018.

[6] R. Piazza, B. S. M. R. Rao, and B. Ottersten, "Data predistortion for multicarrier satellite channels using orthogonal memory polynomials," in *Proc. IEEE 14th Workshop Signal Process. Adv. Wireless Commun. (SPAWC)*, Darmstadt, Germany, Jun. 2013, pp. 689–693.

[7] H. Zhang, Y. Zhang, C. Huang, Y. Yuan, and L. Cheng, *Spacecraft Electromagnetic Compatibility Technologies*. Singapore: Springer, 2020.

[8] J. Christensen, "ITU regulations for Ka-band satellite networks," in *Proc. 30th AIAA Int. Commun. Satell. Syst. Conf.*, Ottawa, ONT, Canada, Sep. 2012, pp. 524–527.

[9] H. Fenech, S. Amos, A. Tomatis, and V. Soumpholphakdy, "High throughput satellite systems: An analytical approach," *IEEE Trans. Aerosp. Electron. Syst.*, vol. 51, no. 1, pp. 192–202, Jan. 2015.

[10] M. Vladimirescu, R. Kwiatkowski, and K. Engel, "Tunnel conduction consequences in high frequency microcontacts; passive intermodulation effect," in *Proc. 50th IEEE Holm Conf. Electr. Contacts 22nd Int. Conf. Electr. Contacts Electr. Contacts*, Seattle, WA, USA, Sep. 2004, pp. 152–159.

[11] J. Russer, A. Ramachandran, A. Cangellaris, and P. Russer, "Phenomenological modeling of passive intermodulation (PIM) due to electron tunneling at metallic contacts," in *Int. Microw. Symp. Dig.*, San Francisco, CA, USA, Jun. 2006, pp. 1132–1192.

[12] S. Zhang, X. Zhao, F. Gao, and Y. He, "Study of metal contact resistance and its statistical correlationship with passive intermodulation," in *Proc. IEEE Holm Conf. Electr. Contacts*, Albuquerque, NM, USA, Oct. 2018, pp. 353–358.

[13] J. R. Wilkerson, K. G. Gard, A. G. Schuchinsky, and M. B. Steer, "Electro-thermal theory of intermodulation distortion in lossy microwave components," *IEEE Trans. Microw. Theory Techn.*, vol. 56, no. 12, pp. 2717–2725, Dec. 2008.

[14] R. U. Tariq, M. Ye, L. Chen, Z. Cao, and Y. He, "Novel cost-effective passive intermodulation measurement technique using a single power amplifier," *Measurement*, vol. 176, May 2021, Art. no. 109118.

[15] *Passive RF and Microwave Devices, Intermodulation Level Measurement, International Electrotechnical Commission (IEC)*, Standard IEC62037, 2012.

[16] M. Alizadeh and D. Rönnow, "A two-tone test for characterizing nonlinear dynamic effects of radio frequency amplifiers in different amplitude regions," *Measurement*, vol. 89, pp. 273–279, Jul. 2016.

[17] P. L. Lui, "Passive intermodulation interference in communication systems," *Electron. Commun. Eng. J.*, vol. 2, no. 3, pp. 109–118, Jun. 1990.

[18] *Radio-Frequency Channel Arrangements for Low and Medium Capacity Analogue or Digital Fixed Wireless Systems Operating in the 2 GHz Band*, Standard ITU-R F.283-5, 1990.

[19] H. Hausman, "Fundamentals of satellite communications, Part III," Tech. Rep., Dec. 2009. [Online]. Available: https://ieee.li/pdf/viewgraphs/fundamentals_satellite_communication_part_3.pdf

[20] D. D. Weiner and J. F. Spina, *Sinusoidal Analysis and Modeling of Weakly Nonlinear Circuits*. New York, NY, USA: Van Nostrand Reinhold, 1980.

[21] S. Shayegani, J. Salmon, and R. Singh, "Multicarrier PIM behavior and testing in communications satellites," in *Proc. 9th Int. Workshop Multipactor, Corona Passive Intermodulation*, Noordwijk, The Netherlands, Apr. 2017, pp. 1–11.

[22] M. Silicani and S. Ricard, "Presentation of MDA PIM test facility capabilities and studies of PIM order amplitude relationship and PIM level variation as a function of transmit power flux density," in *Proc. 9th Int. Workshop Multipactor, Corona Passive Intermodulation*, Noordwijk, The Netherlands, Apr. 2017, pp. 1–9.

[23] G. H. Schennum and G. Rosati, "Minimizing passive intermodulation product generation in high power satellites," in *Proc. IEEE Aerosp. Appl. Conf.*, Aspen, CO, USA, Feb. 1996, pp. 155–164.

[24] C. Vicente, D. Wolk, H. L. Hartnagel, B. Gimeno, V. E. Boria, and D. Raboso, "Experimental analysis of passive intermodulation at waveguide flange bolted connections," *IEEE Trans. Microw. Theory Techn.*, vol. 55, no. 5, pp. 1018–1028, May 2007.

[25] D. Smacchia et al., "Advanced compact setups for passive intermodulation measurements of satellite hardware," *IEEE Trans. Microw. Theory Techn.*, vol. 66, no. 2, pp. 700–710, Feb. 2018.

[26] D. Smacchia, P. Soto, V. E. Boria, D. Raboso, and M. Guglielmi, "Comparison of third order passive inter-modulation products in two and three high power RF carriers scenarios," in *Proc. 9th Int. Workshop Multipactor, Corona Passive Intermodulation*, Noordwijk, The Netherlands, Apr. 2017, pp. 1–8.

[27] D. Smacchia, P. Soto, V. E. Boria, and D. Raboso, "A new model to determine passive intermodulation terms when non-contributing carriers are added to classical scenarios," *IEEE Access*, vol. 9, pp. 152070–152074, 2021.

[28] *MATLAB*. Mathworks, Natick, MA, USA. Accessed: Apr. 2024. [Online]. Available: https://www.mathworks.com/products/matlab.html

[29] D. Smacchia, "Advanced techniques for the characterization and experimental validation of passive inter-modulation (PIM) in space communication systems," Ph.D. dissertation, Departamento de Comunicaciones, Universitat Politècnica de València, Valencia, Spain, Mar. 2022.

Davide Smacchia was born in Fano, Italy, in 1982. He received the B.S. and M.S. degrees (cum laude) in electronic engineering from the Università di Perugia, Perugia, Italy, in 2005 and 2008, respectively, and the Ph.D. degree (cum laude) in telecommunications engineering from the Universitat Politècnica de València, Valencia, Spain, in 2022.

From 2008 to 2010, he was a Researcher with the Departamento de Comunicaciones, Universitat Politècnica de València, granted by a Generalitat Valenciana Santiago Grisolia Fellowship. In 2010, he joined the European Space Agency (ESA)-Val Space Consortium (VSC) European High Power RF Space Laboratory, Valencia. His research interests include RF breakdown phenomena, such as multipactor and corona, as well as the analysis and measurement of passive intermodulation (PIM) for both conducted and radiated scenarios.

Dr. Smacchia is a member of the Val Space Consortium Research and Development Board and of the Technical Committee of the International Workshop on Multipactor, Corona and Passive Intermodulation (Mulcopim).

Pablo Soto (Member, IEEE) was born in Cartagena, Spain, in 1975. He received the M.S. degree and Ph.D. degree (cum laude) in telecommunication engineering from the Universitat Politècnica de València, Valencia, Spain, in 1999 and 2012, respectively.

In 2000, he joined the Departamento de Comunicaciones, Universitat Politècnica de València, where he has been an Associate Professor, since 2012. He was a European Union Research Fellow with the European Space Research and Technology Centre (ESTEC-ESA), Noordwijk, the Netherlands, in 2000. His research interests include numerical methods for analysis, synthesis, and fully automated design of passive components in waveguide technology, the development and design of novel hardware for satellite applications, and the characterization and mitigation of high-power RF effects.

Vicente E. Boria (Fellow, IEEE) was born in Valencia, Spain, in May 1970. He received the Ingeniero de Telecomunicación (Hons.) and Doctor Ingeniero de Telecomunicación degrees from the Universitat Politècnica de València, Valencia, in 1993 and 1997, respectively.

In 1993, he joined the Departamento de Comunicaciones Universitat Politècnica de València, where he has been a Full Professor, since 2003. In 1995 and 1996, he held a Spanish Trainee position with the European Space Research and Technology Centre, European Space Agency (ESTEC-ESA), Noordwijk, the Netherlands, where he was involved in the area of EM analysis and design of passive waveguide devices. He has authored or coauthored 15 chapters in technical textbooks, 200 papers in refereed international technical journals, and over 250 papers in international conference proceedings. His current research interests are focused on the analysis and automated design of passive components (in particular filters and multiplexers) in several technologies, as well as on the simulation and measurement of power effects in high-frequency devices and systems.

Dr. Boria has been a member of the IEEE Microwave Theory and Techniques Society (IEEE MTT-S) and IEEE Antennas and Propagation Society (IEEE AP-S), since 1992. He is also a member of the European Microwave Association (EuMA) and has been the Chair of the 48th European Microwave Conference held in Madrid, Spain. He acts as a Regular Reviewer of the most relevant IEEE and IET technical journals on his areas of interest. He has been the Associate Editor of IEEE MICROWAVE AND WIRELESS COMPONENTS LETTERS (2013–2018) and *IET Electronics Letters* (2015–2018). Presently, he serves as Subject Editor (Microwaves) for *IET Electronics Letters*, and as the Editorial Board Member of the *International Journal of RF and Microwave Computer-Aided Engineering*. He is also a member of the Technical Committees of the IEEE-MTT International Microwave Symposium and the European Microwave Conference.

Òscar Monerris received the M.S. degree in electrical engineering from the Universitat Politecnica de Valencia, Valencia, Spain, in 2008, the M.S. degree in economics from the Universitat de Valencia, Valencia, in 2014, and the Ph.D. degree in electrical engineering from the Universitat Politecnica de Valencia in 2023.

Since 2010, he has been an integral part of the Val Space Consortium, concentrating on high-power RF effects in space applications. Recognized for his expertise, he has served on the Consortium's Research and Development Board, since 2020. Additionally, he has contributed significantly to the Telecommunication Engineering Association Board in Valencia, since 2016, showcasing his commitment to interdisciplinary collaboration and advancement in both engineering and economics.

Javier Ossorio was born in Valencia, Spain, in March 1992. He received the M.S. and Ph.D. degrees in telecommunications engineering from the Universitat Politècnica de València, Valencia, Spain, in 2014 and 2021, respectively.

In 2021, he joined Val Space Consortium, where he is currently a Technical Staff involved in the measurement of high-power effects on RF hardware for space applications. His current research interests include EM simulation, efficient design and optimization of waveguide filters, development of new tunable structures, and high-power effects on RF/microwave components.

David Raboso was born in Alcazar de San Juan, Spain, in 1967. He received the M.S. degree in physics from the Autonomous University of Madrid, Madrid, Spain, in 1992. In 2002, he received the master's degree in space engineering from the University of Delft, Delft, the Netherlands.

In 1992, he joined the Payloads Systems Division, European Space Agency (ESA), Noordwijk, the Netherlands, where he became responsible for all activities related to RF breakdown and PIM in microwave space components. His participation in space programs is extensive, from pioneer observation satellites to modern interplanetary missions. He was granted the Telecommunications Engineer Honoris Causa at the Universitat Politècnica de València, Valencia, Spain, in 2018. Since 1994, he has been the Chairperson of the international conference covering issues of RF breakdown and passive intermodulation (Mulcopim) as well as ESA's responsible for updating the standards related to this discipline. Presently, he manages the joint ESA-VSC European laboratories in high-power RF and space materials in Valencia.

José Vicente Morro was born in Segorbe, Spain, in 1978. He received the Ingeniero de Telecomunicación and Doctor Ingeniero de Telecomunicación degrees from the Universitat Politècnica de València, Valencia, Spain, in 2001 and 2011, respectively.

In 2001, he became a Research Assistant with the Universitat Politècnica de València. In 2003, he joined the Area de Teoría de la Señal y Comunicaciones, Universidad Miguel Hernández de Elche, Elche, Spain, where he was a Lecturer from 2003 to 2005. In 2005, he rejoined the Departamento de Comunicaciones, Universitat Politècnica de València as an Assistant Lecturer, as a Lecturer from 2007, and since 2016, he has been an Assistant Professor. His current research interests include the synthesis and automated design of passive components in waveguides, planar and hybrid technologies, additive manufacturing, and EM optimization methods.

Mónica Martínez-Mendoza was born in Cartagena, Spain, in 1983. She received the Telecommunications Engineer degree from the Universidad Politécnica de Cartagena (UPCT), Cartagena, in 2006, and the Ph.D. degree from Universidad Politécnica de Cartagena (UPCT) under NPI Initiative with European Space Agency (ESA) in 2011.

In 2007, she joined the Telecommunication and Electromagnetic Group, UPCT, as a Research Assistant. From 2008 to 2010, she was with the Payload Systems Division, European Space Research and Technology Centre (ESTEC), ESA, Noordwijk, the Netherlands, where she continued her work on microwave filter synthesis and analysis as a Young Graduate Trainee. In 2012, she was with the Universitat Politècnica de València (UPV), Valencia, Spain, where she was involved with the synthesis and design of multiplexers. From 2013 to 2015, she was granted a Post-Doctoral Humboldt Research Fellowship to work on the synthesis and design of reconstruction filters for Class-S power amplifiers at the Ferdinand-Braun-Institut (FBH), Berlin, Germany. In 2016, she joined Thales Alenia Space, Madrid, Spain, where she was responsible for RF passive equipment design from initial concept up to delivered products for satellite programs for six years. From 2023, she works as a Researcher at UPV. Her current scientific interests include the analysis and design of microwave circuits for satellite applications as well as the analysis of passive intermodulation (PIM).